



1     **Measurement Report: Rapid changes of chemical characteristics and health risks for high**  
2     **time-resolved trace elements in PM<sub>2.5</sub> in a typical industrial city in response to stringent**  
3     **clean air actions**

4             Rui Li<sup>a\*</sup>, Meng Peng<sup>b,c\*</sup>, Weidong Zhao<sup>c\*</sup>, Gehui Wang<sup>a</sup>, Jiming Hao<sup>b</sup>

5     <sup>a</sup> *Key Laboratory of Geographic Information Science of the Ministry of Education, School of*  
6     *Geographic Sciences, East China Normal University, Shanghai, 200241, P.R. China*

7     <sup>b</sup> *State Key Joint Laboratory of Environment Simulation and Pollution Control, School of*  
8     *Environment, Tsinghua University, Beijing, 100084, P.R. China*

9     <sup>c</sup> *Institute of energy conservation and environmental protection, China Electronic Information*  
10     *Industry Development Research Institute, Beijing, 100084, P.R. China*

11     **\* Correspondence to:**

12     Prof. Li ([rli@geo.ecnu.edu.cn](mailto:rli@geo.ecnu.edu.cn)), Dr. Peng ([mvponesky@163.com](mailto:mvponesky@163.com)), and Prof. Zhao  
13     ([zhaoweidong@ccidthinktank.com](mailto:zhaoweidong@ccidthinktank.com))

14     **Abstract**

15     Atmospheric trace metals entail significant damages in human health and ecosystem safety, and  
16     thus a series of clean air actions have been implemented to decrease the ambient metal  
17     concentrations. Unfortunately, the impact of these emission control measures on element  
18     concentrations in fine particles remained poorly understood. In our study, the random forest (RF)  
19     model was applied to distinguish the effects of emission and meteorology to trace elements in PM<sub>2.5</sub>  
20     in a typical industrial city named Tangshan based on a three-year (2017-2020) hourly field  
21     observation. The result suggested that the clean air actions have facilitated the dramatic decreases  
22     of the deweathered concentrations of Ga, Co, Pb, Zn, and As by 72%, 67%, 62%, 59%, and 54%,  
23     respectively. It is attributable to the strict implementation of “coal to gas” strategies and  
24     optimization of industrial structure and layout. However, the deweathered levels of Ca (8.3%), Cr  
25     (18.5%), and Fe (23%) only displayed minor decreases, indicating that the emission control  
26     measures for ferrous metal smelting and vehicle emission were not very effective. The positive  
27     matrix factorization (PMF) results suggested that the contribution ratios of biomass burning, non-



28 ferrous metal smelting, coal combustion, ferrous metal smelting, heavy oil combustion, and traffic-  
29 related dust changed from 5%, 17%, 20%, 15%, 9%, and 34% to 7%, 13%, 15%, 14%, 10%, and  
30 41%, respectively. To date, no significant noncarcinogenic and carcinogenic risks were observed  
31 for all of the elements, while both of As and Pb still showed relatively high health damages. It was  
32 proposed to further cut down the combustion-related emissions (e.g., As and Pb) because it showed  
33 the highest marginal health benefits. Besides, the control of traffic-related emissions might be a key  
34 abatement strategy to facilitate the reduction of elements in fine particles.

35 **Keywords:** hourly trace elements; chemical characteristics; health risks; clean air actions; Tangshan

## 36 1. Introduction

37 Along with the rapid economic development and accelerated urbanization, the energy  
38 consumption and output of various industrial products worldwide displayed the persistent increases,  
39 thereby leading to the massive emissions of elements especially trace metals into the atmosphere  
40 (Tian et al., 2015; Zhu et al., 2020). These elements injected into the atmosphere could pose great  
41 threaten to the terrestrial and aquatic ecosystem via dry/wet deposition and then endanger human  
42 health through the physiochemical transfer and bioaccumulation in food chains (Fernandez et al.,  
43 2000; Harmens et al., 2010; Storelli, 2008). For instance, some toxic trace metals including  
44 cadmium (Cd), lead (Pb), and mercury (Hg) were often regarded as human carcinogens even in trace  
45 amounts (Micheline et al., 2019; Olujimi et al., 2015). Besides, the excessive accumulation of some  
46 biological essential elements such as copper (Cu), iron (Fe), and zinc (Zn) could initiate activation  
47 of inflammatory cascades in tissues and the induction of biochemical synthesis pathways by  
48 catalyzing the generation of reactive oxygen species (ROS) (Alies et al., 2013; Lopez-Cruz et al.,  
49 2016; Saffari et al., 2014), though minor enrichment of these elements was beneficial to the human  
50 health and plant growth (Oldani et al., 2017). Apart from the health impacts, some transition metals  
51 (e.g., Ni, Zn) could catalyze some chemical reactions such as particle-phase sulfate generation and  
52 heterogeneous production and removal of gas-phase hydrogen oxide radicals (HO<sub>x</sub>) to aggravate the  
53 haze formation (Clements et al., 2013; Guo et al., 2014). Therefore, it is highly imperative to  
54 recognize the pollution status of elements in the atmosphere, to identify the major sources and then  
55 to propose effective controls measures to alleviate their negative effects on air pollution and human  
56 health especially in some developing countries.



57 In the past decades, hundreds of studies investigated the pollution levels of elements and  
58 revealed their sources in various study regions including urban (Das et al., 2018; Duan and Tan,  
59 2013; Lyu et al., 2017), marine (Shi et al., 2015; Witt et al., 2006), mountain (Kang et al., 2016).  
60 Most of these studies used the filter sampling (one sample or two samples each day) technique  
61 coupled with offline analysis using inductively coupled plasma mass spectrometry (ICP-MS) or  
62 inductively coupled plasma-atomic emission spectrometry (ICP-AES) to determine the element  
63 concentrations in the atmosphere (Ao et al., 2019; Lin et al., 2016). Although these studies have  
64 obtained many valuable information about the occurrence levels and key sources of ambient  
65 elements, the low time-resolution data cannot accurately reflect the dynamic transformation and  
66 evolution of ambient elements. It was well known that atmospheric emissions, transport and  
67 deposition significantly relied on rapidly evolving meteorological conditions (Holden et al., 2016;  
68 Rasmussen, 1998), and thus the offline samples inevitably ignored the impacts of environmental  
69 shifts with rapid temporality on the atmospheric element concentrations. Moreover, most of current  
70 source apportionment studies employed the receptor models (positive matrix factorization (PMF))  
71 to determine the potential sources of elements (Jeong et al., 2016; Lyu et al., 2017), and the accuracy  
72 of these models was strongly dependent on the sample size and time resolution (Liu et al., 2018b).  
73 In this regard, the high time-resolved observation of atmospheric elements provided an  
74 unprecedented opportunity to characterize the occurrence levels, identify their major sources, and  
75 assess the health impacts.

76 To date, only a few studies applied the high-resolution devices to capture the hourly variability  
77 of ambient elements. Dall'Osto et al. (2013) firstly employed Particle Induced X-ray Emission  
78 (PIXE) measurements to analyze the hourly trace metals in Barcelona, Spain during 20 September-  
79 20 October 2010. Later on, Jeong et al. (2016) used Xact metals monitor to reveal the temporal  
80 variability of atmospheric elements in Toronto, Canada in summer and winter during 2013-2014.  
81 Recently, the Xact metals monitor has begun to be performed in China due to the higher accuracy  
82 and convenience. Chang et al. (2018) firstly used the online multi-element analyzer to achieve a  
83 one-year near real-time observation of ambient elements in China and found traffic, nonferrous  
84 metal smelting and coal combustion were major sources of atmospheric trace metals. Afterwards,  
85 Cui et al. (2019) applied the analyzer to monitor 1-year atmospheric elements, and demonstrated



86 that dust, industry, and biomass burning were considered as the dominant sources of most trace  
87 elements in Beijing, accounting for 36%, 10.7%, and 27% of total PM<sub>2.5</sub> concentration, respectively.  
88 Up to date, continuous hourly element observation was only performed less than one year in most  
89 of the previous studies, and the long-term temporal variability of absolute concentrations and key  
90 pollution sources of atmospheric elements cannot be fully revealed.

91 Since 2013, Chinese government proposed strict Air Pollution Prevention and Control Action  
92 Plan (the Action Plan) across China and the emissions of multiple gaseous pollutants suffered from  
93 significant decreases. In turn, the absolute concentrations and health effects of air pollutants also  
94 experienced the rapid changes response to these stringent control measures. Zhang et al. (2019)  
95 reported that the population-weighted annual mean PM<sub>2.5</sub> concentration decreased from 62 to 42  
96 µg/m<sup>3</sup> during 2013-2017 and reduced PM<sub>2.5</sub>-attributable premature deaths by 0.4 million due to the  
97 impact of the Action Plan. Shortly after that, Geng et al. (2019) estimated that the population-  
98 weighted mean concentrations of SO<sub>4</sub><sup>2-</sup>, NO<sub>3</sub><sup>-</sup>, and NH<sub>4</sub><sup>+</sup> in PM<sub>2.5</sub> decreased from 11.1, 13.8, and  
99 7.4 µg/m<sup>3</sup> to 6.7, 13.1, and 5.8 µg/m<sup>3</sup>, respectively during the same period. Nevertheless, the impact  
100 of the Action Plan on trace elements in fine particles still remained poorly understood. Especially,  
101 the knowledge about the variation of source apportionment and health risks for trace elements  
102 response to the Action Plan was extremely limited. Moreover, most of the previous studies only  
103 utilized the original concentrations to analyze the impact of clean air policy (He et al., 2021; Xiao  
104 et al., 2020). It was well known that the pollutant concentrations in the atmosphere were affected  
105 by meteorology and anthropogenic emissions simultaneously (Li et al., 2021), and the use of original  
106 element concentrations alone cannot assess the unique contribution of emission reduction to the air  
107 pollutants. Thus, it is urgently needed to remove the effect of meteorology and accurately capture  
108 the independent influence of the Action Plan on the chemical characteristics, source apportionment,  
109 and health risks of trace elements. Such knowledge is critical to design effective air pollution  
110 mitigation strategies in the near future.

111 As a heavily industrialized city located in North China Plain (NCP), Tangshan possesses many  
112 energy-intensive industries including coal-fired power plants, non-ferrous smelting industries,  
113 textiles, building materials, chemical engineering, and papermaking industries (Ren et al., 2011).  
114 Intensifying industrial development and urbanization aggravated local air quality. Previous studies



115 performed in Tangshan focused on the trace metals in soils and dusts (Cui et al., 2020; Song et al.,  
116 2011), whereas no study analyzed the long-term and high-resolution variabilities of atmospheric  
117 elements. Since 2013, many emission control measures such as the establishment of desulfurization  
118 and denitration facilities for coal-fired power sector have been strictly implemented in Tangshan  
119 (Ma et al., 2019). Especially after 2017, coal to gas project has started to be implemented in  
120 Tangshan and the energy structure suffered from significant change (Wang et al., 2020b). In  
121 response to substantial pollution control policies, the chemical compositions and major sources of  
122 trace elements might show corresponding change. Here, we conducted a near real-time  
123 measurement of atmospheric elements in  $PM_{2.5}$  using a Xact multi-metals analyzer in Tangshan,  
124 China during September 2017 to August 2020. The primary objectives of our study were to (1)  
125 determine the occurrence levels of elements in  $PM_{2.5}$  of Tangshan; (2) to analyze the seasonal and  
126 intra-week variations of atmospheric elements and to distinguish the separate contributions of  
127 emission and meteorology to these species; (3) to quantify the changes of major sources for  
128 atmospheric elements during this period; (4) to assess the changes of health risks in response to  
129 these pollution control measures.

## 130 **2. Material and methods**

### 131 2.1 Sampling site

132 The sampling site (39.66°N, 118.18°E) is situated on the rooftop (~20 m above the ground) of a  
133 building in the urban district of Tangshan and no high buildings spread around within 100 m range.  
134 The sampling site is close to some major roads including Airport Road, Huayan North Road, and  
135 Changhong Road. A large number of commercial streets and recreation facility surround the site.  
136 Although no big industrial point source was closely adjacent to the sampling site, many potential  
137 pollution sources were located more than 15 km away from the site. For instance, Beihu industrial  
138 region is located about 15 km in the eastern direction of the site. Some large iron steel industries  
139 and nonferrous/ferrous smelting industries were located on the north of sampling site (more than 30  
140 km). Besides, most of large petrochemical industries, coal-fired power plants, and shipping  
141 industries focus on Caofeidian and Haigang developing zones, both of which were located about 50  
142 km in the South area of the sampling site. The detailed location is depicted in Figure 1.

### 143 2.2 Instrumentation



144 Hourly mass concentrations of 22 elements, including Ag, As, Au, Ca, Co, Cu, Cd, Cr, Fe, Ga,  
145 Hg, K, Mn, Ni, Pb, Pd, Sb, Se, Sn, Tl, V, and Zn in  $PM_{2.5}$  were determined by an online multi-  
146 element analyzer (Model Xact 625, Cooper Environment Service, USA). The sample air is drawn  
147 through a small spot on the tape where the  $PM_{2.5}$  was collected at a flow rate of  $16.7 \text{ L min}^{-1}$  during  
148 September 2017-August 2020. An internal Pd pod is utilized as an internal standard to detect the  
149 stability of the instrument. Tl was removed from the datasets because over 95% of their  
150 concentrations were below the limit of detection (LOD) (Table S1). Au, Cd, Sn and Sb were also  
151 excluded from the datasets because over 50% of the concentrations for these metals were below the  
152 LOD. To validate the reliability of online multi-element analyzer, many previous studies used the  
153 filter sampling coupled with ICP-MS and ICP-AES to determine the daily concentrations of  
154 elements and confirmed that the online device showed good agreement with the filter sampling  
155 (Furger et al., 2017; Tianxue et al., 2006). Hourly averaged meteorological parameters including air  
156 temperature (T), relative humidity (RH), air pressure (P), wind direction (WD), and wind speed  
157 (WS) during the sampling period were also measured.

### 158 2.3 Deweathered model development

159 The concentrations of air pollutants were affected by meteorological parameters and emissions  
160 simultaneously. In order to separate the contributions of emissions, the impacts of meteorological  
161 conditions must be eliminated. In this study, a typical machine-learning model named random forest  
162 (RF) approach was applied to distinguish the effects of emissions and meteorological conditions  
163 (Chen et al., 2018). All of trace elements in  $PM_{2.5}$  were treated as the dependent variables. The time  
164 predictors (year, day of year (DOY), day of week (DOW), hour of day (HOY)) and meteorological  
165 factors including air temperature (T), relative humidity (RH), wind speed (WS), wind direction  
166 (WD), and air pressure (P) were regarded as the predictors (Figure S1). The original dataset was  
167 randomly classified into a training dataset (80% of input dataset) for developing the RF model and  
168 the remained one was treated as the test dataset. After the building of the RF model, the deweathered  
169 technique was employed to predict the concentrations of trace elements at a specific time point. The  
170 deweathered element concentrations served as the concentrations contributed by emission alone.  
171 The differences of original element concentrations and deweathered element concentrations were  
172 regarded as the concentrations contributed by meteorology. Many statistical indicators including  $R^2$



173 value, RMSE, and MAE were regarded as the major indicators to evaluate the RF modelling  
174 accuracy. The RF model with the 5-fold cross-validation  $R^2$  value less than 0.5 was considered to  
175 be the unconvincing result and cannot reflect the impacts of emission and meteorology on air  
176 pollutants accurately because more than 50% variability of the training model cannot be  
177 appropriately explained. After the model evaluation, only the trace elements with the cross-  
178 validation  $R^2$  values larger than 0.5 were selected to estimate the respective contributions of  
179 emission and meteorology to the total element concentrations.

#### 180 2.4 PMF model

181 As a typical receptor model applied to source apportionment, PMF 5.0 version was used to  
182 identify the major origins of atmospheric elements and to determine the contribution ratio of each  
183 source to these elements. The objective of PMF is to solve the issues of chemical mass balance  
184 between measured concentration of each element and its source contributions by decomposing the  
185 input matrix into factor contribution and factor profile. The detailed equation is shown in Eq. (1).  
186 Besides, the contribution of each source for individual element must be non-negative because no  
187 sample has a negative source contribution. In brief, the basic principle of PMF is to calculate the  
188 least object function  $Q$  when the  $g_{ik}$  must be a positive-definite matrix based on Eq. (2) (Paatero and  
189 Tapper, 1994; Reff et al., 2007).

$$190 \quad x_{ij} = \sum_{k=1}^p g_{ik} f_{kj} + e_{ij} \quad (1)$$

$$191 \quad Q = \sum_{i=1}^n \sum_{j=1}^m \left[ \frac{x_{ij} - \sum_{k=1}^p g_{ik} f_{kj}}{u_{ij}} \right]^2 \quad (2)$$

192 where  $x_{ij}$  and  $e_{ij}$  denote the concentration and uncertainty of  $j$ th element, respectively.  $g_{ik}$  represents  
193 the contribution ratio of  $k$ th source to  $i$ th sample,  $f_{kj}$  represents the ratio of  $j$ th element in  $k$ th source,  
194 and  $e_{ij}$  indicates the residual of  $j$ th element in the  $i$  sample. The uncertainties associated with factor  
195 profiles were evaluated using three error calculation methods including bootstraps (BS) method,  
196 displacement (DISP) analysis, and the combination method of DISP and BS (BS-DISP). For the BS  
197 method, 100 runs were performed and the result has been believed to be valid since all of the factors  
198 showed a mapping of above 90%. DISP analysis also confirmed that the solution was considered to  
199 be stable because the observed drop in the  $Q$  value was less than 0.1% and no factor swap occurred.



200 For the BS-DISP analysis, the solution has been verified to be useful because the observed drop in  
201 the Q value was less than 0.5%. Furthermore, both of the results from BS and BS-DISP did not  
202 suggest any asymmetry or rotational ambiguity for all of the factors (Manousakas et al., 2017;  
203 Taghvaei et al., 2018).

#### 204 2.5 Health risk assessment of trace metals in PM<sub>2.5</sub>

205 As a typical industrial city, Tangshan possesses a large number of residents and poor air quality.  
206 Therefore, the residents in Tangshan might suffer from severe exposure risks of trace metals. In our  
207 work, the carcinogenic and non-carcinogenic risks of trace metals in PM<sub>2.5</sub> were evaluated based on  
208 some statistical threshold proposed by International Agency for Research on Cancer (IARC). Based  
209 on the criterion of IARC, As, Ni, Cr, and Pb were considered to be carcinogenic to humans.

210 The carcinogenic and non-carcinogenic risks induced by metal exposure for adults and children  
211 were evaluated based on the carcinogenic risks (CR) and hazard quotient (HQ). The formulas for  
212 calculating ADD, CR, and HQ are as follows:

$$213 \quad \text{ADD} = (C \times \text{InhR} \times \text{EF} \times \text{ED}) / (\text{BW} \times \text{AT}) \quad (3)$$

$$214 \quad \text{HQ} = \text{ADD} / \text{RfD} \quad (4)$$

$$215 \quad \text{CR} = \text{ADD} \times \text{CSF} \quad (5)$$

216 where C (mg m<sup>-3</sup>) denotes the concentration of the corresponding trace metal in PM<sub>2.5</sub>; InhR is the  
217 respiratory rate; EF represents the annual exposure frequency (d y<sup>-1</sup>); ED is the exposure duration;  
218 BW is the average body weight; AT denotes the average exposure time; ADD means the daily intake  
219 (mg/kg/day) of trace metals; RfD represents the reference dose, calculated with reference  
220 concentrations; CSF is the cancer slope factor. The non-carcinogenic risk of the trace metal is  
221 considered to be high when HQ was above 1, whereas the health risk is not obvious when HQ is  
222 below 1. The carcinogenic risk of each trace metal is evaluated based on whether CR is higher than  
223 10<sup>-4</sup>.

### 224 3. Results and discussion

#### 225 3.1 Occurrence levels and inter-annual variations of original element concentrations

226 The total mass concentrations of 16 elements in PM<sub>2.5</sub> of Tangshan varied between 230 ng/m<sup>3</sup>  
227 to 20000 ng/m<sup>3</sup>, with the median value of 3100 ± 900 ng/m<sup>3</sup>. The total element concentrations in  
228 Tangshan accounted for 5.7% of the total mass concentrations of PM<sub>2.5</sub>, which was slightly higher





229 than those in Beijing (4.7%) and Qingdao (4.0%), and significantly higher than that in Shanghai  
230 (1.80%) (Chang et al., 2018; Cui et al., 2019). As depicted in Figure 2, the concentrations of these  
231 elements followed the order of K ( $1400 \pm 950 \text{ ng/m}^3$ ) > Fe ( $880 \pm 590 \text{ ng/m}^3$ ) > Ca ( $330 \pm 270$   
232  $\text{ng/m}^3$ ) > Zn ( $320 \pm 160 \text{ ng/m}^3$ ) > Pb ( $58 \pm 36 \text{ ng/m}^3$ ) > Mn ( $54 \pm 32 \text{ ng/m}^3$ ) > Cu ( $22 \pm 19 \text{ ng/m}^3$ ) >  
233 As ( $15.3 \pm 11.0 \text{ ng/m}^3$ ) > Se ( $6.5 \pm 5.3 \text{ ng/m}^3$ ) > V ( $4.0 \pm 3.6 \text{ ng/m}^3$ ) > Cr ( $2.8 \pm 2.2 \text{ ng/m}^3$ ) > Ag  
234 ( $2.8 \pm 2.1 \text{ ng/m}^3$ ) > Ni ( $2.2 \pm 1.8 \text{ ng/m}^3$ ) > Hg ( $1.5 \pm 0.8 \text{ ng/m}^3$ ) > Ga ( $0.9 \pm 0.7 \text{ ng/m}^3$ ) > Co ( $0.7 \pm$   
235  $0.2 \text{ ng/m}^3$ ). Among all of these elements, K, Fe, Zn, and Ca were most abundant species, accounting  
236 for 95% of the total elements in  $\text{PM}_{2.5}$ . The remaining element concentrations only accounted for  
237 less than 6% of the total element concentrations, which was similar to the previous studies (Chang  
238 et al., 2018; Cui et al., 2019).

239 Due to the higher exposure risk and great threaten to human health, it is necessary to compare  
240 the trace metal concentrations with the risk threshold proposed by many organizations or countries.  
241 As shown in Table 1, we have collected many risk thresholds in different countries and found that  
242 the Hg ( $1.5 \pm 0.8 \text{ ng/m}^3$ ), Ni ( $2.2 \pm 1.8 \text{ ng/m}^3$ ), and Pb concentrations ( $58 \pm 36 \text{ ng/m}^3$ ) in Tangshan  
243 were significantly lower than the thresholds of the Chinese Ambient Air Quality Standard (CAAQS)  
244 (Hg:  $50 \text{ ng/m}^3$ ), World Health Organization (WHO) (Hg:  $1000 \text{ ng/m}^3$ , Ni:  $25 \text{ ng/m}^3$ , and Pb:  $1000$   
245  $\text{ng/m}^3$ ), Europe Union (EU) (Ni:  $20 \text{ ng/m}^3$ ), and the United States (Pb:  $150 \text{ ng/m}^3$ ). However, both  
246 of the As ( $15 \pm 11 \text{ ng/m}^3$ ) and Cr concentrations ( $2.8 \pm 2.2 \text{ ng/m}^3$ ) in  $\text{PM}_{2.5}$  of Tangshan were much  
247 higher than the standard values of CAAQS (As:  $6.0 \text{ ng/m}^3$  and Cr:  $0.03 \text{ ng/m}^3$ ), WHO (As:  $6.6 \text{ ng/m}^3$   
248 and Cr:  $0.3 \text{ ng/m}^3$ ), and EU (As:  $6.0 \text{ ng/m}^3$ ).

249 The inter-annual variation of original concentrations of trace elements in  $\text{PM}_{2.5}$  are depicted in  
250 Figure 3. The original concentrations of all the trace elements exhibited the decreasing trends. Cu,  
251 Co, Zn, Pb, As, and Ga concentrations suffered from dramatic decreases from 37 to  $12 \text{ ng/m}^3$  (68%),  
252  $1.21$  to  $0.4 \text{ ng/m}^3$  (66%),  $400$  to  $190 \text{ ng/m}^3$  (53%),  $71$  to  $40 \text{ ng/m}^3$  (44%),  $20$  to  $11 \text{ ng/m}^3$  (44%), and  
253  $1.09$  to  $0.6 \text{ ng/m}^3$  (42%), respectively. Following these species, observed K (40%), Ag (39%), V  
254 (39%), Ni (36%), Ca (33%), Mn (29%), Se (29%), Fe (27%), and Cr (21%) concentrations showed  
255 moderate decreasing ratios. The observed Hg level exhibited the lowest decreasing ratio from  $1.59$   
256 to  $1.43 \text{ ng/m}^3$  (9.9%).

257 3.2 Impact of emission reduction on trace element concentrations



258 Although the original concentrations of trace elements could be utilized to analyze the impact of  
259 the clean air policy, the role of emission reduction on element concentration might not be clearly  
260 clarified because the meteorological factors were also important variables affecting the air quality.  
261 In order to accurately reflect the response of element concentrations to emission reduction alone  
262 during 2017-2020, the meteorological conditions were eliminated by RF model in our study. Based  
263 on the results in Figure S2, the RF models for all of the species showed better performance because  
264 their  $R^2$  values were higher than 0.5, and the slopes of all of the fitting curves were also close to the  
265  $R^2$  values. The result suggested that the separation of meteorology and emission of trace elements  
266 based on RF model was reliable. During 2017-2020, the deweathered concentrations of Ga, Co, Pb,  
267 Zn, and As showed the rapid decreases from 1.52 to 0.4 ng/m<sup>3</sup> (72%), 1.31 to 0.4 ng/m<sup>3</sup> (67%), 92  
268 to 35 ng/m<sup>3</sup> (62%), 410 to 170 ng/m<sup>3</sup> (59%), and 21 to 10 ng/m<sup>3</sup> (54%), respectively (Figure 3). It  
269 was well known that As, Co, and Pb were typical marker elements for coal combustion and the  
270 “coal-to-gas” and “coal-to-electricity” strategies have been widely performed in Tangshan (Fang et  
271 al., 2020; Li et al., 2017). Wang et al. (2020a) has estimated that these effective control measures  
272 have contributed to around 60% of the total PM<sub>2.5</sub> reductions. Meanwhile, the upgradation and  
273 optimization of industrial structure/layout and the shutdown of high-pollution industries were also  
274 strictly implemented in Tangshan, and thus led to the dramatic decreases of Ga and Zn  
275 concentrations because Ga and Zn were common forms of nonferrous metal smelting (Tian et al.,  
276 2015). However, the deweathered Ca level displayed the lowest decrease ratio (8.3%) from 2017 to  
277 2020, indicating that clean air actions cannot significantly reduce the fugitive emissions. In addition,  
278 the deweathered Fe (23%) and Cr (18.5%) also suffered from relatively low decrease ratios. It was  
279 well documented that Fe and Cr originated from metallurgical industry such as steel production and  
280 ferrous metal smelting (Tian et al., 2015), and the slight decreases of deweathered Fe and Cr levels  
281 during the sampling period suggested that the emission control measures for ferrous metal smelting  
282 should be strengthened in the future work.

283 In addition, the reduction ratios of the deweathered concentrations for each species displayed  
284 different seasonal characteristics. The deweathered concentrations of some elements related with  
285 industrial activities (e.g., Ga, Zn, and Cr) suffered from rapid decreases in autumn and winter  
286 compared with other seasons during 2017-2020 (Figure 4), indicating that the optimization of



287 industrial layout and shutdown of outdated industries were effective to decrease these element  
288 emissions especially in high-pollution season. Some elements derived from biomass burning  
289 including K (66%) and Se (50%) also suffered from the most dramatic decreasing ratios in autumn.  
290 It was assumed that enhanced crop residual burning occurred frequently during the autumn harvest  
291 season. However, the control on open biomass burning has been implemented strictly in recent years,  
292 largely reducing the K and Se emissions in autumn. It should be noted that the deweathered Pb  
293 (46%), Co (65%), and As (45%) concentrations in winter did not display high decreasing ratios  
294 though the annual mean deweathered Pb, Co and As levels experienced dramatic decreases. The  
295 result revealed that it was still difficult to reduce the Pb, Co, and As emissions during the heating  
296 season because increased coal consumption for domestic heating largely offset the contributions of  
297 emission control measures.

298 Apart from the seasonal difference of each species, the decreasing ratios of these elements also  
299 suffered from distinctly intra-weekly variations. The deweathered concentrations of most elements  
300 except Ca, Cu, Ni, and V exhibited the higher decreasing ratios at the weekends than those in the  
301 weekdays (Figure 5). Cui et al. (2020) has demonstrated that the weaker supervision on industrial  
302 enterprises on weekends could lead to the higher concentrations of non-traffic elements such as K,  
303 As, Se, and Cr in some cities. Fortunately, grid monitoring has been widely performed in Tangshan  
304 recently, and many low-cost sensors were installed at some energy-intensive industries, which could  
305 decrease the stealing emissions of some elements. Nonetheless, the decreasing ratios of Ca, Cu, V,  
306 and Ni did not show the regular intra-weekly characteristics. In recent years, Tangshan adopted  
307 strict traffic management regulation and the nonlocal light duty vehicles were restricted to drive  
308 inside the urban area one day per week based on the end number of the license plates (Westerdahl  
309 et al., 2009; Wu et al., 2011), whereas the restrictions were not valid at weekends (Liu et al., 2007).  
310 Theoretically, the traffic control should result in marked decreases of traffic-related element  
311 concentrations on weekdays compared with weekends. However, in our study, some traffic-related  
312 elements such as Ca and Cu did not show similar characteristics. It was supposed that the vehicle  
313 volume in Tangshan has increase from 2.0 to 2.4 million (<http://tjj.hebei.gov.cn/>), which largely  
314 offset the benefits of traffic controls. The shipping-related elements including Vi and Ni also did  
315 not show regular intra-weekly variation because no similar emission control measures for shipping



316 were performed.

### 317 3.3 The role of meteorology on the year-to-year variations of element concentrations

318 The difference of original and deweathered element concentrations could be regarded as the  
319 concentrations contributed by meteorological parameters. The positive impacts of meteorological  
320 parameters on trace elements suggested that the meteorological conditions were unfavorable to the  
321 pollutant diffusion, while the negative impacts of meteorological indicators meant the favorable  
322 condition to trace elements. In our study, the roles of meteorological conditions on Ca (-25%), V (-  
323 10%), Cr (-2.5%), Mn (-0.7%), Fe (-4.6%), Ni (-7.6%), and Cu (-21%) during 2017-2020 were  
324 negative (Figure S3), while the roles of meteorological parameters on other elements were positive.  
325 The result suggested that those elements derived from vehicle emission (Ca, Cu, and Fe), ferrous  
326 metal smelting (Cr and Mn), and heavy oil combustion (V and Ni) were less sensitive to the emission  
327 reduction actions compared with other elements and the meteorological conditions were much  
328 beneficial to the diffusion of these elements. In order to further reveal the key meteorological factors  
329 for these elements, we used RF model to calculate the variable importance of all of these  
330 meteorological parameters including P, RH, T, WD, and WS. The result suggested that Ca, Fe, and  
331 Cu were mainly influenced by T, whereas V, Ni, Cr, and Mn were often associated with WD and  
332 WS (Figure 6). During 2017-2020, the average air temperature increased from 14.2 to 14.6 °C. The  
333 elevated air temperature was often favorable to the advection and convection of particulate matter,  
334 and might decrease the concentrations of Ca, Fe, and Cu (Manju et al., 2018; Yang et al., 2017).  
335 Although the annual average wind speed in Tangshan decreased from 1.70 to 1.45 m/s, the mean  
336 wind speed from the southeastern direction displayed slight increase from 1.34 to 1.50 m/s. Zhao et  
337 al. (2013) verified that V and Ni were usually emitted from heavy oil combustion of ocean-going  
338 ship engines. Many coastal ports and ferrous metal smelting industries were located on the  
339 southeastern direction of the sampling site, and thus the enhanced WS promoted the dilution and  
340 dispersion of trace elements.

### 341 3.4 The impact of clean air policy on source apportionment of trace elements

342 Although the major sources of elements could be determined based on some important tracers  
343 (e.g., K, V), the contributions of major sources to each element still remained unknown. Therefore,  
344 Positive matrix factorization (PMF 5.0) version was applied to identify more source information of



345 elements in  $PM_{2.5}$  during 2017-2018, 2018-2019, and 2019-2020 based on deweathered levels. After  
346 20 runs, more than 26000 samples were trained to determine the optimal six factors with the lowest  
347 values of  $Q$  (robust) and  $Q$  (true). The BS, DISP, and BS-DISP methods confirmed that the most  
348 reliable solution was obtained with six factors. The detailed information of PMF analysis and error  
349 diagnostics are summarized in Table S2-4.

350 As shown in Figure S4-6, the trace elements in  $PM_{2.5}$  during 2017-2018, 2018-2019, and 2019-  
351 2020 showed similar cluster characteristics. Factor 1 possesses high loadings of K (53% (2017-  
352 2018), 55% (2018-2019), and 58% (2019-2020)) and Se (40%, 42%, and 44%). K and Se were often  
353 regarded as the major tracers of biomass burning. Due to the increasing usage of biomass fuels for  
354 domestic heating during the heating season, K, and Se in  $PM_{2.5}$  of Tangshan showed the higher  
355 values in winter, suggesting that these metals in fine particles could originate from the combustion  
356 of biomass fuels. Except the domestic heating, we found some episodes during harvesting season in  
357 late summer and early autumn also showed extremely high concentrations of K, which might be  
358 linked with open biomass burning (Chen et al., 2017). Based on the map of fire points and backward  
359 air masses trajectories (Figure S7), the metals released from biomass burning or open waste  
360 incineration in NCP could be transported to the sampling site by the dominant southerly wind, which  
361 further proved the impacts of open biomass burning (Chen et al., 2017).

362 The abundant elements in factor 2 included Ag (55%, 52%, and 51%), Zn (54%, 52%, and 48%),  
363 and Cu (37%, 35% and 35%). Owing to the higher temperatures during the roasting, sintering and  
364 smelting processes for the extraction of Cu, and Zn from ores, some metals such Ag in nonferrous  
365 metal ores could be vaporized as the byproduct and released into the flue gas (Pacyna and Pacyna,  
366 2001; Wu et al., 2012). Therefore, the factor 2 was interpreted as the nonferrous metal smelting  
367 source.

368 Factor 3 was characterized by a large mass fraction of Co (86%, 80%, and 78%), Pb (66%, 60%,  
369 and 57%), Hg (63%, 55%, and 52%), and As (41%, 38%, and 37%). After the phase-out of leaded  
370 gasoline since 1980s, the contribution from coal combustion to Pb suffered from rapid increase and  
371 accounted for the major fraction of particulate Pb (Das et al., 2018). Meanwhile, Co and Hg were  
372 also treated as the important byproducts released from coal burning and the Co and Hg  
373 concentrations often increased significantly with the elevation of burning temperature (Tang et al.,



374 2018). Tian et al. (2015) estimated that 73% of As, 56 % of Pb, and 47 % of Hg were found to be  
375 emitted from coal combustion in China. Coal consumption in South China was mainly driven by  
376 coal-fired power plants, while the coal-based heating was the major sector for the coal consumption  
377 in NCP. In our study, As, Co and Pb showed the higher concentrations in winter (heating season)  
378 compared with other seasons. The markedly seasonal discrepancies of As, Co and Pb strongly  
379 supported the impact of the coal combustion for domestic heating on the enhancement of As, Co  
380 and Pb in the fine particles.

381 Factor 4 was distinguished by high loadings of Cr (81%, 77% and 75%) and Mn (43%, 40% and  
382 35%), respectively. Cr and Mn were mainly sourced from metallurgical industry such as steel  
383 production and ferrous metal smelting (Liu et al., 2018a; Tian et al., 2015; Zhu et al., 2018). China  
384 occupied more than 49% of world steel production in 2017 (approximate 830 million tons), and 60%  
385 large steel producers were located in China (Chang et al., 2018). Tangshan possesses many large  
386 steel production industries such as Tangshan Steel, Qian'an Steel, and Guofeng Steel. Besides, some  
387 industries of Capital Steel have been migrated into Tangshan (Li et al., 2019), which might increase  
388 the Cr and Mn emissions. As depicted in Figure S8, these metals emitted from steel production  
389 industries could be transported over substantial distances to the sampling site. The presence of  
390 ferrous metal smelting activities located in the northern direction of the sampling site was inferred  
391 to be associated with the accumulation of Cr and Mn in  $PM_{2.5}$ .

392 Factor 5 explained 9.3% of the total species and it was characterized by high loadings of V (87%,  
393 88%, and 88%) and Ni (49%, 51%, and 54%). It was well documented that V was a key fingerprint  
394 of heavy oil combustion, which was generally emitted from shipping emission and petrochemical  
395 refining (Shafer et al., 2012). However, Ni was widely utilized as a tracer of fuel oil combustion in  
396 industries (Zhu et al., 2018). Many oil-fired power plants were located in Tangshan for central  
397 heating (Yu et al., 2013). Based on the backward trajectory and wind direction (Figure S7 and S9),  
398 we found that high concentrations of V and Ni might be derived from the southeastern air masses  
399 especially in summer and autumn, indicating the impacts of coastal port and petroleum refinery  
400 industry. Gathering evidence suggested that the V/Ni ratio in petroleum coke with a low-sulfur  
401 content and fuel oil usage ranged from 1 to 3 (Moreno et al., 2010). The annual mean ratios of V  
402 and Ni in our study reached 1.2, which was in the range of this interval. The result also revealed that



403 petrochemical refining and combustion might be an important source of V and Ni the fine particles.

404 Factor 6 was characterized by high loadings of Ca (75%, 79%, and 81%), Cu (30%, 33%, and  
405 33%), and Fe (30%, 34%, and 35%), and moderate loadings of Mn (29%, 30%, and 34%) and Zn  
406 (27%, 29%, and 32%). Some previous studies have demonstrated that both of Cu, Fe, and Zn were  
407 released from tyre and brake wear because they were the necessary materials for brake pads and the  
408 agents in brake linings (Dall'Osto et al., 2013; Hjortenkrans et al., 2007). Ca was probably sourced  
409 from the road fugitive dust because it was one of the most abundant elements in the upper continents  
410 (Alves et al., 2015; Liu et al., 2018a). Moreover, we have found Fe, Ca, and Zn displayed  
411 remarkably high values during the rush hours, which was coincident to the diurnal variation of traffic  
412 volume. Thus, the factor 6 was identified as the traffic-related dust source.

413 Although six similar sources were revealed during 2017-2018, 2018-2019, and 2019-2020, the  
414 contribution ratios of these sources varied greatly in these years. As shown in Figure 7, the  
415 contribution ratios of traffic-related dust and biomass burning increased from 34% to 40% and 5%  
416 to 8%, respectively. However, the contributions of non-ferrous metal smelting and coal combustion  
417 decreased from 17% to 13% and 20% to 15%, respectively. The contributions of ferrous metal  
418 smelting and heavy oil combustion remained relatively stable during this period. Due to the strict  
419 implementation of clean air policy, many outdated industrial capacity was shut down and the cleaner  
420 technologies have been upgraded, which facilitated the production decreases of pig iron and coal-  
421 fired power plants. Hence, the contributions of non-ferrous metal smelting and coal combustion  
422 experienced dramatic decreases. The loadings of Co, Hg, and Pb suffered from dramatic decreases  
423 from 86% to 80%, 63% to 55%, and 66% to 60%, respectively. It was assumed that these elements  
424 were closely linked with coal combustion. Although the open biomass burning has been strictly  
425 restricted in Tangshan (Chang et al., 2018), the contribution ratios of biomass burning to trace  
426 elements in PM<sub>2.5</sub> still showed the slight increases, which might be attributable to the rapid decreases  
427 of the contributions derived from coal combustion and non-ferrous metal smelting. In addition, the  
428 biofuel combustion was still widespread in some rural and suburb areas (Kamal et al., 2015; Li et  
429 al., 2020), which might offset the decreases in the contributions of open biomass burning. The  
430 contributions of traffic-related dust to some trace elements such as Ca (75% to 81%), Fe (30% to  
431 35%), and Zn (27% to 32%) exhibited the marked increases during 2017-2020 because the



432 contributions of metal smelting and coal combustion suffered from rapid decreases. Moreover, the  
433 formulation of many new quality standards for non-road diesel fuels cannot fully decrease the  
434 element emissions (Cui et al., 2017), and thus the traffic-related dust was regarded as the major  
435 contributor to the trace elements in  $PM_{2.5}$  in Tangshan.

#### 436 3.4 Health risk assessment of trace metals in $PM_{2.5}$

437 Although the trace metals only accounted for minor fraction of total mass concentration of  $PM_{2.5}$ ,  
438 it might pose a great threaten to the human health because most of these metals were bioavailable  
439 and non-degradable (Rai et al., 2019; Yi et al., 2011). Unfortunately, previous studies mainly used  
440 the filter sampling techniques to determine the concentrations of trace metals and then assess their  
441 health risks (Cui et al., 2018; Huang et al., 2016). These low-resolution data might not accurately  
442 reflect the real health risks triggered by metal exposure. In our study, we employed the online data  
443 to assess the health risks derived from metal exposure.

444 The health risks of trace metals could be classified into two types including carcinogenic and  
445 non-carcinogenic risk. Based on the major parameters summarized in Table S5 and Table S6, we  
446 estimated both of the carcinogenic and non-carcinogenic risks of major metals. To evaluate the  
447 impacts of emission control measures on element concentrations, both of the health risks based on  
448 original element levels and deweathered element concentrations were calculated. The mean CR  
449 values based on original concentrations were in the order of Pb ( $2.3 \times 10^{-6}$  (adult) and  $1.4 \times 10^{-6}$   
450 (child)) > As ( $1.9 \times 10^{-6}$  and  $1.1 \times 10^{-6}$ ) > Cr ( $0.11 \times 10^{-6}$  and  $0.10 \times 10^{-6}$ ). The total CR values for adults  
451 and children reached  $4.3 \times 10^{-6}$  and  $2.6 \times 10^{-6}$  (Table 2), respectively. The total CR values were located  
452 in the range of the acceptable ( $10^{-6}$ ) and least stringent risk levels ( $10^{-4}$ ), which suggested that  
453 Tangshan suffered from slight metal carcinogenic risk. Among all of these metals, Pb and As  
454 displayed the higher CR values. It was assumed that the coal combustion for domestic heating might  
455 be the dominant factor for the higher risks of Pb and As in Tangshan because both of Pb and As in  
456  $PM_{2.5}$  were mainly derived from coal combustion. With regard to the non-carcinogenic risks of trace  
457 metals, the HQ of As ( $1.2 \times 10^{-2}$  and  $2.9 \times 10^{-2}$ ) and Pb ( $6.8 \times 10^{-4}$  and  $17 \times 10^{-4}$ ) showed the higher  
458 values compared with other elements. The result indicated that nearly all of the elements did not  
459 display remarkable non-carcinogenic risk because HQ values of all the metals were less than 1. The  
460 total HQ value of these metals were also lower than 1, indicating that the trace elements in Tangshan





461 did not show significant non-carcinogenic risk.

462 By removing the impact of meteorological conditions, we can isolate the impact of clean air  
463 policy on health risks associated with metal exposure alone. The decrease ratios of CR values based  
464 on the deweathered As and Pb concentrations during 2017-2020 were 54% and 62%, respectively  
465 (Table 3). However, the decrease ratios of CR values based on original As and Pb levels only  
466 reached 44%. The result suggested that the clean air policy in recent years significantly decreased  
467 the As and Pb emissions. Additionally, the decrease ratios of HQ values for original Cu (41%) and  
468 Zn (53%) were much less than those for deweathered ones (Cu: 47% and Zn: 59%). Nevertheless,  
469 some other elements did not show the similar characteristics. For instance, the decrease ratios of  
470 HQ values for original Cr (21%) and Fe (27%) were even slightly higher than those for deweathered  
471 ones (Cr: 19% and Fe: 23%). It was assumed that the clean air policy in recent years facilitated the  
472 emission reduction of non-ferrous metal smelting and coal combustion efficiently. However, the  
473 concentrations of elements derived from ferrous metal smelting and vehicle emission did not show  
474 marked decreases, which was in good agreement with the source apportionment result in the section  
475 3.3. Thus, in the future work, it is highly imperative to further reduce the industrial/traffic-related  
476 emissions in order to alleviate potential health risks.

#### 477 **4. Conclusions and implications**

478 Three-year continuous hourly observation of elements in PM<sub>2.5</sub> was conducted in Tangshan  
479 during September 2017-August 2020. The effect of air clean policy on element concentrations in  
480 PM<sub>2.5</sub> were quantified. The main conclusions were drawn as follows:

- 481 (1) The deweathered concentrations of Ga, Co, Pb, Zn, and As showed the rapid decreases from  
482 1.52 to 0.42 ng/m<sup>3</sup> (72%), 1.31 to 0.44 ng/m<sup>3</sup> (67%), 92 to 35 ng/m<sup>3</sup> (62%), 411 to 170 ng/m<sup>3</sup>  
483 (59%), and 21 to 10 ng/m<sup>3</sup> (54%), respectively. Clean air actions played the important role on  
484 the emission reduction of coal combustion and non-ferrous metal smelting.
- 485 (2) The deweathered levels of Ca (8.3%), Cr (19%), and Fe (23%) displayed relatively low  
486 decreases compared with other elements, indicating that the vehicle emission and ferrous-  
487 smelting industries might be not sensitive to the air clean policy.
- 488 (3) The deweathered levels of some elements related with industrial activities (e.g., Ga, Zn, and Cr)  
489 exhibited rapid decreases in autumn and winter compared with other seasons during 2017-2020,



490 while the combustion-related elements such as Pb and As did not show high decreasing ratios  
491 in winter. The enhanced coal consumption during the heating season offset the benefits derived  
492 from strict emission controls measures.

493 (4) The favorable meteorological conditions promoted the decreases of Ca (-25%), V (-10%), Cr (-  
494 2.6%), Mn (-0.68%), Fe (-4.6%), Ni (-7.6%), and Cu (-21%) concentrations.

495 (5) The contribution ratios of biomass burning, non-ferrous metal smelting, coal combustion,  
496 ferrous metal smelting, heavy oil combustion, and traffic-related dust changed from 5%, 17%,  
497 20%, 15%, 9%, and 34% to 7%, 13%, 15%, 14%, 10%, and 41%, respectively.

498 (6) All of the elements did not show significant noncarcinogenic and carcinogenic risks, while both  
499 of As and Pb still displayed relatively high health damages.

500 Our study presented detailed information about the impact of clean air policy on the chemical  
501 compositions and source apportionment of trace elements in PM<sub>2.5</sub> in Tangshan, and provided new  
502 enlightenment for scientific community and policymakers. Many targeted measures could be  
503 undertaken to alleviate the air pollution and further to reduce avoided premature health risks.  
504 However, this study still suffered some limitations and more steps will be taken toward thoroughly  
505 addressing these problems. First of all, the PMF model still showed some uncertainties, and thus  
506 characterizing the isotopic signatures of these elements is of great significance. In addition, Sunset  
507 OC/EC analyzer, Monitoring of Aerosols and Gases (MARGA) platform, and other on-line  
508 measurements should be collocated to probe into the synergistic effect of emission reduction and  
509 meteorology on air quality.

#### 510 **Acknowledgements**

511 This work was supported by the National Natural Science Foundation of China (42107113).

#### 512 **Data availability**

513 The boundary layer height dataset was obtained from the website of <https://www.ecmwf.int/>. The  
514 dataset is archived in <https://zenodo.org/record/7031975#.Ywys8cjfmFU> (Li et al., 2022).

#### 515 **Author contributions**

516 LR wrote the manuscript. LR, PM, ZWD, and HJM contributed to the conceptualization of the study.

517 LR and PM conducted the research, and visualized the results. WGH revised the manuscript.

#### 518 **Competing interests**



519 The contact author has declared that neither they nor their co-authors have any competing interests.



520 **References**

- 521 Alies, B., Sasaki, I., Proux, O., Sayen, S., Guillon, E., Faller, P., and Hureau, C.: Zn impacts Cu  
522 coordination to amyloid- $\beta$ , the Alzheimer's peptide, but not the ROS production and the associated  
523 cell toxicity. *Chem. Commun.*, 49, 1214-1216, 2013.
- 524 Alves, C., Gomes, J., Nunes, T., Duarte, M., Calvo, A.I., Custodio, D., Pio, C., Karanasiou, A., and  
525 Querol, X.: Size-segregated particulate matter and gaseous emissions from motor vehicles in a road  
526 tunnel. *Atmos. Res.*, 153, 134-144, <https://doi.org/10.1016/j.atmosres.2014.08.002>, 2015.
- 527 Ao, M., Qiu, G., Zhang, C., Xu, X., Zhao, L., Feng, X., Qin, S., and Meng, B.: Atmospheric deposition  
528 of antimony in a typical mercury-antimony mining area, Shaanxi Province, Southwest China. *Environ.*  
529 *Pollut.*, 245, 173-182, <https://doi.org/10.1016/j.envpol.2018.10.125>, 2019.
- 530 Chang, Y., Huang, K., Xie, M., Deng, C., Zou, Z., Liu, S., and Zhang, Y.: First long-term and near real-  
531 time measurement of trace elements in China's urban atmosphere: temporal variability, source  
532 apportionment and precipitation effect. *Atmos. Chem. Phys.*, 18, 11793-11812,  
533 <https://doi.org/10.5194/acp-18-11793-2018>, 2018.
- 534 Chen, J., Li, C., Ristovski, Z., Milic, A., Gu, Y., Islam, M.S., Wang, S., Hao, J., Zhang, H., and He, C.: A  
535 review of biomass burning: Emissions and impacts on air quality, health and climate in China. *Sci.*  
536 *Total Environ.*, 579, 1000-1034, <https://doi.org/10.1016/j.scitotenv.2016.11.025>, 2017.
- 537 Chen, G.B., Li, S.S., Knibbs, L.D., Hamm, N.A.S., Cao, W., Li, T.T., Guo, J.P., Ren, H.Y., Abramson,  
538 M.J., and Guo, Y.M.: A machine learning method to estimate PM<sub>2.5</sub> concentrations across China with  
539 remote sensing, meteorological and land use information. *Sci. Total Environ.*, 636, 52-60,  
540 <https://doi.org/10.1016/j.scitotenv.2018.04.251>, 2018.
- 541 Clements, A.L., Buzcuguvan, B., Fraser, M.P., Kulkarni, P., and Chellam, S.: Role of particulate metals  
542 in heterogenous secondary sulfate formation. *Atmos. Environ.*, 75, 233-240,  
543 <https://doi.org/10.1016/j.atmosenv.2013.04.038>, 2013.
- 544 Cui, L., Duo, B., Zhang, F., Li, C., Fu, H., and Chen, J.: Physiochemical characteristics of aerosol  
545 particles collected from the Jokhang Temple indoors and the implication to human exposure. *Environ.*  
546 *Pollut.*, 236, 992-1003, <https://doi.org/10.1016/j.envpol.2017.10.107>, 2018.
- 547 Cui, M., Chen, Y., Feng, Y., Li, C., Zheng, J., Tian, C., Yan, C., and Zheng, M.: Measurement of PM and  
548 its chemical composition in real-world emissions from non-road and on-road diesel vehicles. *Atmos.*  
549 *Chem. Phys.*, 17, 6779-6795, <https://doi.org/10.5194/acp-17-6779-2017>, 2017.
- 550 Cui, X., Wang, X., and Liu, B.: The characteristics of heavy metal pollution in surface dust in Tangshan,  
551 a heavily industrialized city in North China, and an assessment of associated health risks. *J. Geochem.*  
552 *Explor.*, 210, 106432, 2020.
- 553 Cui, Y., Ji, D., Chen, H., Gao, M., Maenhaut, W., He, J., and Wang, Y.: Characteristics and sources of  
554 hourly trace elements in airborne fine particles in urban Beijing, China. *J. Geophys. Res. Atmos.*, 124,  
555 11595-11613, <https://doi.org/10.1029/2019JD030881>, 2019.
- 556 Dall'Osto, M., Querol, X., Amato, F., Karanasiou, A., Lucarelli, F., Nava, S., Calzolari, G., and Chiari,  
557 M.: Hourly elemental concentrations in PM<sub>2.5</sub> aerosols sampled simultaneously at urban background  
558 and road site during SAPUSS -diurnal variations and PMF receptor modelling. *Atmos. Chem. Phys.*,  
559 13, 4375-4392, 2013.
- 560 Das, R., Mohtar, A.T.B.M., Rakshit, D., Shome, D., and Wang, X.: Sources of atmospheric lead (Pb) in  
561 and around an Indian megacity. *Atmos. Environ.*, 193, 57-65,  
562 <https://doi.org/10.1016/j.atmosenv.2018.08.062>, 2018.



- 563 Duan, J. and Tan, J.: Atmospheric heavy metals and arsenic in China: situation, sources and control  
564 policies. *Atmos. Environ.*, 74, 93-101, 10.1016/j.atmosenv.2013.03.031, 2013.
- 565 Fang, B., Zhang, L., Zeng, H., Liu, J., Yang, Z., Wang, H., Wang, Q., and Wang, M.: PM<sub>2.5</sub>-bound  
566 polycyclic aromatic hydrocarbons: sources and health risk during non-heating and heating periods  
567 (Tangshan, China). *Int. J. Env. Res. Pub. He.*, 17, 483, 2020.
- 568 Fernandez, J.A., Rey, A., and Carballeira, A.: An extended study of heavy metal deposition in Galicia  
569 (NW Spain) based on moss analysis. *Sci. Total Environ.*, 254, 31-44, 10.1016/s0048-9697(00)00431-  
570 9, 2000.
- 571 Furger, M., Minguillon, M.C., Yadav, V., Slowik, J.G., Hüglin, C., Frohlich, R., Petterson, K.,  
572 Baltensperger, U., and Prevot, A.S.H.: Elemental composition of ambient aerosols measured with high  
573 temporal resolution using an online XRF spectrometer. *Atmos. Meas. Technol.*, 10, 2061-2076,  
574 <https://doi.org/10.5194/amt-10-2061-2017>, 2017.
- 575 Geng, G., Xiao, Q., Zheng, Y., Tong, D., Zhang, Y., Zhang, X., Zhang, Q., He, K., and Liu, Y.: Impact of  
576 China's air pollution prevention and control action plan on PM<sub>2.5</sub> chemical composition over eastern  
577 China. *Sci. China Earth Sci.*, 62, 1872-1884, <https://doi.org/10.1007/s11430-018-9353-x>, 2019.
- 578 Guo, J., Tilgner, A., Yeung, C., Wang, Z., Louie, P.K.K., Luk, C.W.Y., Xu, Z., Yuan, C., Gao, Y., and  
579 Poon, S.: Atmospheric peroxides in a polluted subtropical environment: seasonal variation, sources  
580 and sinks, and importance of heterogeneous processes. *Environ. Sci. Technol.*, 48, 1443-1450,  
581 <https://doi.org/10.1021/es403229x>, 2014.
- 582 Harmens, H., Norris, D.A., Steinnes, E., Kubin, E., Piispanen, J., Alber, R., Aleksiyenak, Y., Blum, O.,  
583 Coskun, M., and Dam, M.: Mosses as biomonitors of atmospheric heavy metal deposition: Spatial  
584 patterns and temporal trends in Europe. *Environ. Pollut.*, 158, 3144-3156,  
585 <https://doi.org/10.1016/j.envpol.2010.06.039>, 2010.
- 586 He, Q., Zhang, M., Song, Y., and Huang, B.: Spatiotemporal assessment of PM<sub>2.5</sub> concentrations and  
587 exposure in China from 2013 to 2017 using satellite-derived data. *J. Cleaner Prod.*, 286, 124965,  
588 <https://doi.org/10.1016/j.jclepro.2020.124965>, 2021.
- 589 Hjortenkran, D.S., Bergbäck, B.G., and Häggerud, A.V.: Metal emissions from brake linings and tires:  
590 case studies of Stockholm, Sweden 1995/1998 and 2005. *Environ. Sci. Technol.*, 41, 5224-5230,  
591 <https://doi.org/10.1021/es070198o>, 2007.
- 592 Holden, P.A., Gardeatorresdey, J.L., Klaessig, F., Turco, R.F., Mortimer, M., Hundrinke, K., Hubal,  
593 E.A.C., Avery, D., Barcelo, D., and Behra, R.: Considerations of environmentally relevant test  
594 conditions for improved evaluation of ecological hazards of engineered nanomaterials. *Environ. Sci.*  
595 *Technol.*, 50, 6124-6145, <https://doi.org/10.1021/acs.est.6b00608>, 2016.
- 596 Huang, C., Bao, L., Luo, P., Wang, Z., Li, S., and Zeng, E.Y.: Potential health risk for residents around a  
597 typical e-waste recycling zone via inhalation of size-fractionated particle-bound heavy metals. *J*  
598 *Hazard. Mater.*, 317, 449-456, 10.1016/j.jhazmat.2016.05.081, 2016.
- 599 Jeong, C., Wang, J.M., and Evans, G.J.: Source apportionment of urban particulate matter using hourly  
600 resolved trace metals, organics, and inorganic aerosol components. *Atmos. Chem. Phys.*, 1-32,  
601 <https://doi.org/10.5194/acp-2016-189>, 2016.
- 602 Kamal, A., Cincinelli, A., Martellini, T., and Malik, R.N.: A review of PAH exposure from the combustion  
603 of biomass fuel and their less surveyed effect on the blood parameters. *Environ. Sci. Pollut. Res.*, 22,  
604 4076-4098, 10.1007/s11356-014-3748-0, 2015.
- 605 Kang, S., Chen, P., Li, C., Liu, B., and Cong, Z.: Atmospheric aerosol elements over the inland Tibetan  
606 Plateau: concentration, seasonality, and transport. *Aerosol Air Qual. Res.*, 16, 789-800, 2016.



- 607 Li, R., Fu, H., Cui, L., Li, J., Wu, Y., Meng, Y., Wang, Y., and Chen, J.: The spatiotemporal variation and  
608 key factors of SO<sub>2</sub> in 336 cities across China. *J. Cleaner Prod.*, 210, 602-611,  
609 <https://doi.org/10.1016/j.jclepro.2018.11.062>, 2019.
- 610 Li, R., Zhao, Y., Fu, H., Chen, J., Peng, M., and Wang, C.: Substantial changes in gaseous pollutants and  
611 chemical compositions in fine particles in the North China Plain during the COVID-19 lockdown  
612 period: anthropogenic vs. meteorological influences. *Atmos. Chem. Phys.*, 21, 8677-8692,  
613 <https://doi.org/10.5194/acp-21-8677-2021>, 2021.
- 614 Li, R., Peng, M., Zhao, W.D., Wang, G.H., and Hao, J.M.: Data for “Measurement Report: Rapid changes  
615 of chemical characteristics and health risks for high time-resolved trace elements in PM<sub>2.5</sub> in a typical  
616 industrial city in response to stringent clean air actions”, [dataset],  
617 <https://zenodo.org/record/7031975#.Ywys8cjfmfU>, 2022.
- 618 Li, Z., Jiang, J., Ma, Z., Fajardo, O.A., Deng, J., and Duan, L.: Influence of flue gas desulfurization (FGD)  
619 installations on emission characteristics of PM<sub>2.5</sub> from coal-fired power plants equipped with selective  
620 catalytic reduction (SCR). *Environ. Pollut.*, 230, 655-662,  
621 <https://doi.org/10.1016/j.envpol.2017.06.103>, 2017.
- 622 Li, Z., Wang, Y., Li, Z., Guo, S., and Hu, Y.: Levels and sources of PM<sub>2.5</sub>-associated pahs during and after  
623 the wheat harvest in a central rural area of the beijing-tianjin-hebei (bth) region. *Aerosol Air Qual.*  
624 *Res.*, 20, 1070-1082, 2020.
- 625 Lin, Y., Hsu, S., Chou, C.C.K., Zhang, R., Wu, Y., Kao, S., Luo, L., Huang, C., Lin, S., and Huang, Y.:  
626 Wintertime haze deterioration in Beijing by industrial pollution deduced from trace metal fingerprints  
627 and enhanced health risk by heavy metals. *Environ. Pollut.*, 208, 284-293,  
628 <https://doi.org/10.1016/j.envpol.2015.07.044>, 2016.
- 629 Liu, H., He, K., Wang, Q., Huo, H., Lents, J., Davis, N., Nikkila, N., Chen, C., Osses, M., and He, C.:  
630 Comparison of vehicle activity and emission inventory between Beijing and Shanghai. *J. Air Waste*  
631 *Manage.*, 57, 1172-1177, <https://doi.org/10.3155/1047-3289.57.10.1172>, 2007.
- 632 Liu, J., Chen, Y., Chao, S., Cao, H., Zhang, A., and Yang, Y.: Emission control priority of PM<sub>2.5</sub>-bound  
633 heavy metals in different seasons: A comprehensive analysis from health risk perspective. *Sci. Total*  
634 *Environ.*, 644, 20-30, <https://doi.org/10.1016/j.scitotenv.2018.06.226>, 2018a.
- 635 Liu, R., Men, C., Yu, W., Xu, F., Wang, Q., and Shen, Z.: Uncertainty in positive matrix factorization  
636 solutions for PAHs in surface sediments of the Yangtze River Estuary in different seasons.  
637 *Chemosphere* 191, 922-936, <https://doi.org/10.1016/j.chemosphere.2017.10.070>, 2018b.
- 638 Lopez-Cruz, J., Crespo-Salvador, O., Fernandez-Crespo, E., Garcia-Agustin, P., and Gonzalez-Bosch, C.:  
639 Absence of Cu-Zn-superoxide dismutase BCSOD1 reduces Botrytis cinerea virulence in Arabidopsis  
640 and in tomato plants, which reveals interplay among ROS, callose and signaling pathways. *Mol. Plant*  
641 *Pathol.*, 18, 16-31, 2016.
- 642 Lyu, Y., Zhang, K., Chai, F., Cheng, T., Yang, Q., Zheng, Z., and Li, X.: Atmospheric size-resolved trace  
643 elements in a city affected by non-ferrous metal smelting: Indications of respiratory deposition and  
644 health risk. *Environ. Pollut.*, 224, 559-571, <https://doi.org/10.1016/j.envpol.2017.02.039>, 2017.
- 645 Ma, Z., Liu, R., Liu, Y., and Bi, J.: Effects of air pollution control policies on PM<sub>2.5</sub> pollution  
646 improvement in China from 2005 to 2017: a satellite-based perspective. *Atmos. Chem. Phys.*, 19,  
647 6861-6877, <https://doi.org/10.5194/acp-19-6861-2019>, 2019.
- 648 Manju, A., Kalaiselvi, K., Dhananjayan, V., Palanivel, M., Banupriya, G., Vidhya, M., Panjakumar, K.,  
649 and Ravichandran, B.: Spatio-seasonal variation in ambient air pollutants and influence of  
650 meteorological factors in Coimbatore, southern India. *Air Qual. Atmos. Heal.*, 11, 1179-1189,



- 651 <https://doi.org/10.1007/s11869-018-0617-x>, 2018.
- 652 Manousakas, M., Papaefthymiou, H., Diapouli, E., Migliori, A., Karydas, A.G., Bogdanovic-Radovic, I.,  
653 and Eleftheriadis, K.: Assessment of PM<sub>2.5</sub> sources and their corresponding level of uncertainty in a  
654 coastal urban area using EPA PMF 5.0 enhanced diagnostics. *Sci. Total Environ.* 574, 155-164, 2017.
- 655 Micheline, G., Rachida, C., Celine, M., Gaby, K., Rachid, A., and Petru, J.: Levels of Pb, Cd, Hg and As  
656 in fishery products from the eastern Mediterranean and human health risk assessment due to their  
657 Consumption. *Interna. J. Environ. Res.*, 13, 443-455, <https://doi.org/10.1007/s41742-019-00185-w>,  
658 2019.
- 659 Moreno, T., Querol, X., Alastuey, A., La Rosa, J.D.D., La Campa, A.M.S.D., Minguillon, M., Pandolfi,  
660 M., Gonzalez-Castanedo, Y., Monfort, E., and Gibbons, W.: Variations in vanadium, nickel and  
661 lanthanoid element concentrations in urban air. *Sci. Total Environ.*, 408, 4569-4579,  
662 <https://doi.org/10.1016/j.scitotenv.2010.06.016>, 2010.
- 663 Oldani, K.M., Mladenov, N., Williams, M., Campbell, C.M., and Lipson, D.A.: Seasonal patterns of dry  
664 deposition at a high-elevation site in the colorado rocky mountains. *J. Geophys. Res. Atmos.*, 122,  
665 2017.
- 666 Olujimi, O.O., Oputu, O., Fatoki, O.S., Opatoyinbo, O.E., Aroyewun, O.A., and Baruani, J.: Heavy  
667 metals speciation and human health risk assessment at an illegal gold mining site in Igun, Osun State,  
668 Nigeria. *J. Health. Pollut.*, 5, 19-32, 2015.
- 669 Paatero, P. and Tapper, U.: Positive matrix factorization: A non-negative factor model with optimal  
670 utilization of error estimates of data values. *Environmetrics* 5, 111-126, 1994.
- 671 Pacyna, J.M. and Pacyna, E.G.: An assessment of global and regional emissions of trace metals to the  
672 atmosphere from anthropogenic sources worldwide. *Environ. Rev.*, 9, 269-298, 2001.
- 673 Rai, P.K., Lee, S.S., Zhang, M., Tsang, Y.F., and Kim, K.: Heavy metals in food crops: Health risks, fate,  
674 mechanisms, and management. *Environ. Interna.*, 125, 365-385, 2019.
- 675 Rasmussen, P.E.: Long-range atmospheric transport of trace metals: the need for geoscience perspectives.  
676 *Environ. Earth Sci.*, 33, 96-108, 1998.
- 677 Reff, A., Eberly, S.I., and Bhave, P.V.: Receptor modeling of ambient particulate matter data using  
678 positive matrix factorization: review of existing methods. *J. Air Waste Manage.*, 57, 146-154, 2007.
- 679 Ren, Z., Zhang, B., Lu, P., Li, C., Gao, L., and Zheng, M.: Characteristics of air pollution by  
680 polychlorinated dibenzo-p-dioxins and dibenzofurans in the typical industrial areas of Tangshan City,  
681 China. *J. Environ. Sci. -China*, 23, 228-235, 2011.
- 682 Saffari, A., Daher, N., Shafer, M.M., Schauer, J.J., and Sioutas, C.: Global perspective on the oxidative  
683 potential of airborne particulate matter: a synthesis of research findings. *Environ. Sci. Technol.*, 48,  
684 7576-7583, 2014.
- 685 Shafer, M.M., Toner, B.M., Overdier, J.T., Schauer, J.J., Fakra, S.C., Hu, S., Herner, J.D., and Ayala, A.:  
686 Chemical speciation of vanadium in particulate matter emitted from diesel vehicles and urban  
687 atmospheric aerosols. *Environ. Sci. Technol.*, 46, 189-195, 2012.
- 688 Shi, G., Teng, J., Ma, H., Li, Y., and Sun, B.: Metals and metalloids in precipitation collected during  
689 CHINARE campaign from Shanghai, China, to Zhongshan Station, Antarctica: Spatial variability and  
690 source identification. *Global Biogeochem. Cyc.*, 29, 760-774, 2015.
- 691 Storelli, M.M.: Potential human health risks from metals (Hg, Cd, and Pb) and polychlorinated biphenyls  
692 (PCBs) via seafood consumption : estimation of target hazard quotients (THQs) and toxic equivalents  
693 (TEQs). *Food and Chemical Toxicology* 46, 2782-2788, 2008.
- 694 Taghvaei, S., Sowlat, M.H., Mousavi, A., Hassanvand, M.S., Yunesian, M., Naddafi, K., and Sioutas, C.:



- 695 Source apportionment of ambient PM<sub>2.5</sub> in two locations in central Tehran using the Positive Matrix  
696 Factorization (PMF) model. *Sci. Total Environ.*, 628-629, 672-686, 2018.
- 697 Tang, Q., Sheng, W., Li, L., Zheng, L., Miao, C., and Sun, R.: Alteration behavior of mineral structure  
698 and hazardous elements during combustion of coal from a power plant at Huainan, Anhui, China.  
699 *Environ. Pollut.*, 239, 768-776, 2018.
- 700 Tian, H., Zhu, C., Gao, J., Cheng, K., Hao, J., Wang, K., Hua, S., Wang, Y., and Zhou, J.: Quantitative  
701 assessment of atmospheric emissions of toxic heavy metals from anthropogenic sources in China:  
702 historical trend, spatial distribution, uncertainties, and control policies. *Atmos. Chem. Phys.*, 15,  
703 10127-10147, 2015.
- 704 Tianxue, W., Yuesi, W., Shihyu, C., and Guangren, L.: On-line measurement of water-soluble ions in  
705 ambient particles. *Adv. Atmos. Sci.*, 23, 586-592, 2006.
- 706 Wang, S., Su, H., Chen, C., Tao, W., Streets, D.G., Lu, Z., Zheng, B., Carmichael, G.R., Lelieveld, J.,  
707 and Pöschl, U.: Natural gas shortages during the “coal-to-gas” transition in China have caused a large  
708 redistribution of air pollution in winter 2017. *P. Natl. Acad. Sci. USA*, 117, 31018-31025, 2020a.
- 709 Wang, S., Su, H., Chen, C., Tao, W., Streets, D.G., Lu, Z., Zheng, B., Carmichael, G.R., Lelieveld, J.,  
710 Pöschl, U., and Cheng, Y.: Natural gas shortages during the “coal-to-gas” transition in China have  
711 caused a large redistribution of air pollution in winter 2017. *P. Natl. Acad. Sci. USA*, 117, 31018-  
712 31025, 2020b.
- 713 Westerdahl, D., Wang, X., Pan, X., and Zhang, K.M.: Characterization of on-road vehicle emission  
714 factors and microenvironmental air quality in Beijing, China. *Atmos. Environ.*, 43, 697-705,  
715 <https://doi.org/10.1016/j.atmosenv.2008.09.042>, 2009.
- 716 Witt, M.L.I., Baker, A.R., and Jickells, T.D.: Atmospheric trace metals over the Atlantic and South Indian  
717 Oceans: Investigation of metal concentrations and lead isotope ratios in coastal and remote marine  
718 aerosols. *Atmos. Environ.*, 40, 5435-5451, <https://doi.org/10.1016/j.atmosenv.2006.04.041>, 2006.
- 719 Wu, Q., Wang, S., Zhang, L., Song, J., Yang, H., and Meng, Y.: Update of mercury emissions from China's  
720 primary zinc, lead and copper smelters, 2000-2010. *Atmos. Chem. Phys.*, 12, 18207-18242,  
721 <https://doi.org/10.5194/acp-12-11153-2012>, 2012.
- 722 Wu, Y., Wang, R., Zhou, Y., Lin, B., Fu, L., He, K., and Hao, J.: On-road vehicle emission control in  
723 beijing: past, present, and future. *Environ. Sci. Technol.*, 45, 147-153,  
724 <https://doi.org/10.1021/es1014289>, 2011.
- 725 Xiao, Q., Geng, G., Liang, F., Wang, X., Lv, Z., Lei, Y., Huang, X., Zhang, Q., Liu, Y., and He, K.:  
726 Changes in spatial patterns of PM<sub>2.5</sub> pollution in China 2000-2018: Impact of clean air policies.  
727 *Environ. Interna.*, 141, 105776, <https://doi.org/10.1016/j.envint.2020.105776>, 2020.
- 728 Yang, Q., Yuan, Q., Li, T., Shen, H., and Zhang, L.: The relationships between PM<sub>2.5</sub> and meteorological  
729 factors in China: seasonal and regional variations. *Int. J. Env. Res. Pub. He.*, 14, 1510, 2017.
- 730 Yi, Y., Yang, Z., and Zhang, S.: Ecological risk assessment of heavy metals in sediment and human health  
731 risk assessment of heavy metals in fishes in the middle and lower reaches of the Yangtze River basin.  
732 *Environ. Pollut.*, 159, 2575-2585, <https://doi.org/10.1016/j.envpol.2011.06.011>, 2011.
- 733 Yu, L., Wang, G., Zhang, R., Zhang, L., Song, Y., Wu, B., Li, X., An, K., and Chu, J.: Characterization  
734 and source apportionment of PM<sub>2.5</sub> in an urban environment in beijing. *Aerosol Air Qual. Res.*, 13,  
735 574-583, doi: 10.4209/aaqr.2012.07.0192, 2013.
- 736 Song, Z.F.: An assessment of the heavy metal pollution and potential ecological hazards in urban soil of  
737 Tangshan City. *Geology in China* 38, 1379-1386, 2011.
- 738 Zhang, Q., Zheng, Y., Tong, D., Shao, M., Wang, S., Zhang, Y., Xu, X., Wang, J., He, H., Liu, W., Ding,





739 Y., Lei, Y., Li, J., Wang, Z., Zhang, X., Wang, Y., Cheng, J., Liu, Y., Shi, Q., Yan, L., Geng, G., Hong,  
740 C., Li, M., Liu, F., Zheng, B., Cao, J., Ding, A., Gao, J., Fu, Q., Huo, J., Liu, B., Liu, Z., Yang, F., He,  
741 K., and Hao, J.: Drivers of improved PM<sub>2.5</sub> air quality in China from 2013 to 2017. P. Natl. Acad. Sci.  
742 USA, 116, 24463-24469, <https://doi.org/10.1073/pnas.1907956116>, 2019.

743 Zhao, M., Zhang, Y., Ma, W., Fu, Q., Yang, X., Li, C., Zhou, B., Yu, Q., and Chen, L.: Characteristics  
744 and ship traffic source identification of air pollutants in China's largest port. Atmos. Environ., 64, 277-  
745 286, <https://doi.org/10.1016/j.atmosenv.2012.10.007>, 2013.

746 Zhu, C., Tian, H., Hao, Y., Gao, J., Hao, J., Wang, Y., Hua, S., Wang, K., and Liu, H.: A high-resolution  
747 emission inventory of anthropogenic trace elements in Beijing-Tianjin-Hebei (BTH) region of China.  
748 Atmos. Environ., 191, 452-462, <https://doi.org/10.1016/j.atmosenv.2018.08.035>, 2018.

749 Zhu, C., Tian, H., and Hao, J.: Global anthropogenic atmospheric emission inventory of twelve typical  
750 hazardous trace elements, 1995-2012. Atmos. Environ., 220, 117061,  
751 <https://doi.org/10.1016/j.atmosenv.2019.117061>, 2020.

752



**Figure 1** The topographic map of China indicating the location of Tangshan (a), sampling site (b), and some major industrial points (b). The population distribution of Tangshan is also depicted in (b).

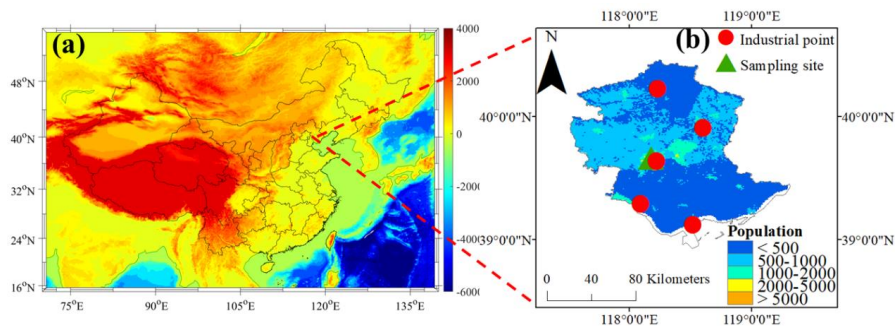




**Figure 2** The bar chart of the concentrations of 16 trace elements including K, Fe, Ca, Zn, Pb, Mn, Fe, As, Se, V, Cr, Ag, Ni, Hg, Ga, and Co.

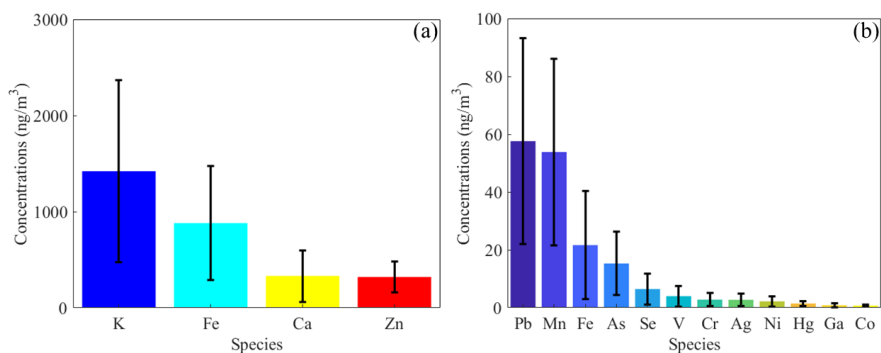




**Figure 3** Inter-annual variations of original (red) and deweathered (manganese purple) element concentrations ( $\text{ng}/\text{m}^3$ ) in  $\text{PM}_{2.5}$  in Tangshan. The dark, nattier blue, and nattier yellow backgrounds represent the species during 2017-2018 (from September in 2017 to August in 2018), 2018-2019 (from September in 2018 to August in 2019), and 2019-2020 (from September in 2019 to August in 2020).

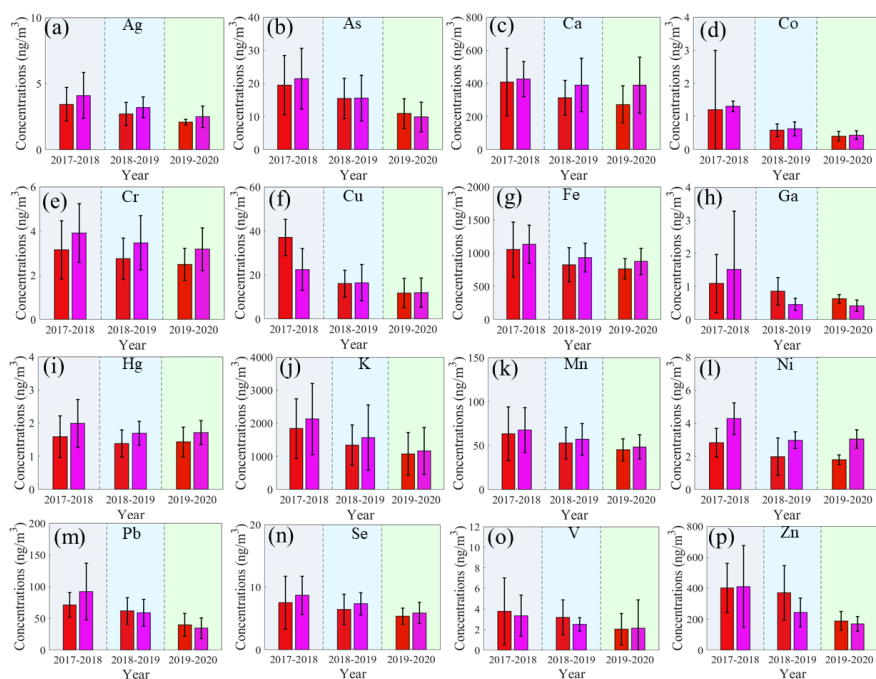




**Figure 4** The original (red and orange) and deweathered (green and blue) element concentrations ( $\text{ng}/\text{m}^3$ ) in  $\text{PM}_{2.5}$  in Tangshan in four seasons during 2017-2018, 2018-2019, and 2019-2020. Spr1, sum1, aut1, and win1 represent the spring, summer, autumn, and winter during 2017-2018. Spr2, sum2, aut2, and win2 denote the spring, summer, autumn, and winter during 2018-2019. Spr3, sum3, aut3, and win3 are the spring, summer, autumn, and winter during 2019-2020.

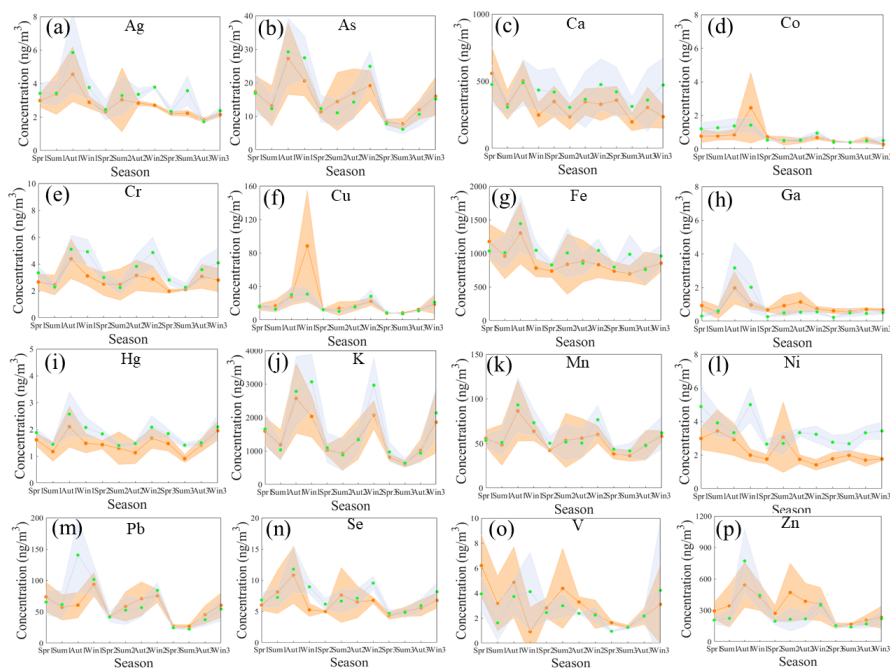




**Figure 5** Weekly variations of original (green) and deweathered (orange) element concentrations ( $\text{ng}/\text{m}^3$ ) in  $\text{PM}_{2.5}$  in Tangshan. The green and dark backgrounds denote the error bars of original and deweathered elements, respectively.

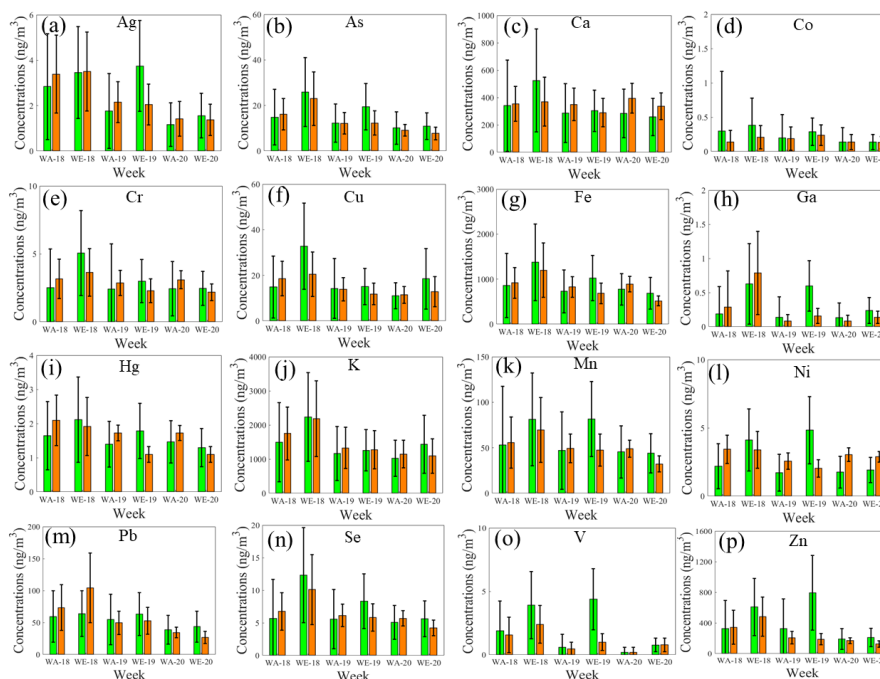




**Figure 6** Relative importance of the predictors for the prediction of trace elements. The columns in the figure represent the variable importance in RF models for trace elements. P, RH, T, WD, WS, DOW, HOY, DOY, and Year denote air pressure, relative humidity, air temperature, wind direction, wind speed, day of week, hour of day, day of year, and study year, respectively.

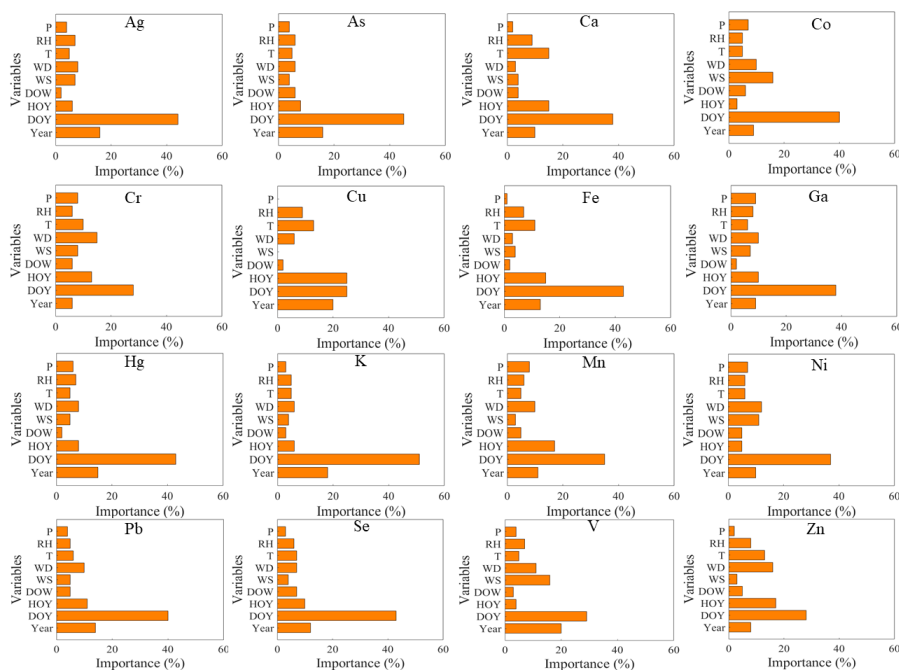




**Figure 7** Average contributions of six sources to the total mass concentrations of metals in PM<sub>2.5</sub>. The red panel means the biomass burning; the green panel denotes the non-ferrous metal smelting; the blue one represents the coal combustion; the cyan one is the ferrous metal smelting; the pink one represents the heavy oil combustion; and the yellow one denotes the traffic-related dust. (a), (b), and (c) represent the source contributions during 2017-2018, 2018-2019, and 2019-2020, respectively.

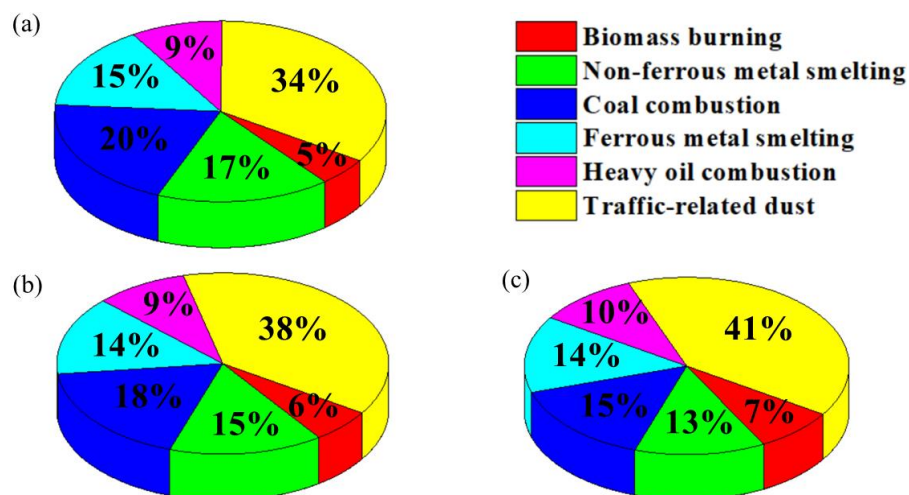






**Table 1** The comparison of element concentrations in PM<sub>2.5</sub> of Tangshan and the standard values for these elements in World Health Organization (WHO), China, Europe, and the United States.

Elements	Mean±SD	CAAQS	WHO	EU	United States
Co	0.74±0.24				
Ga	0.86±0.74				
Hg	1.47±0.81	50	1000		
Ni	2.21±1.80		25	20	
Ag	2.75±2.08				
Cr	2.80±2.22	0.025	0.25		
V	3.98±3.57				
Se	6.46±5.28				
As	15.3±11.0	6	6.60	6	
Cu	21.7±18.7				
Mn	53.8±32.3				
Pb	57.6±35.7		1000		150
Zn	320±162				
Ca	332±268				
Fe	881 ± 591				
K	1421±947				



**Table 2** The non-carcinogenic and carcinogenic risks for the original element levels in PM<sub>2.5</sub>.

Age	Year	Indicator	Cr	Mn	Fe	Co	Ni	Cu	Zn	As	Pb
Adult	2017-2018	HQ	$2.47 \times 10^{-4}$	$1.07 \times 10^{-4}$	$3.55 \times 10^{-4}$	$4.50 \times 10^{-4}$	$0.33 \times 10^{-4}$	$1.18 \times 10^{-4}$	$3.15 \times 10^{-4}$	$1.53 \times 10^{-2}$	$8.39 \times 10^{-4}$
		CR	$0.13 \times 10^{-6}$	--	--	--	--	--	--	$2.37 \times 10^{-6}$	$2.88 \times 10^{-6}$
	2018-2019	HQ	$2.16 \times 10^{-4}$	$0.89 \times 10^{-4}$	$2.77 \times 10^{-4}$	$4.67 \times 10^{-4}$	$0.23 \times 10^{-4}$	$0.95 \times 10^{-4}$	$2.91 \times 10^{-4}$	$1.21 \times 10^{-2}$	$7.28 \times 10^{-4}$
		CR	$0.11 \times 10^{-6}$	--	--	--	--	--	--	$1.87 \times 10^{-6}$	$2.50 \times 10^{-6}$
	2019-2020	HQ	$1.95 \times 10^{-4}$	$0.76 \times 10^{-4}$	$2.58 \times 10^{-4}$	$3.26 \times 10^{-4}$	$0.21 \times 10^{-4}$	$0.70 \times 10^{-4}$	$1.49 \times 10^{-4}$	$0.86 \times 10^{-2}$	$4.69 \times 10^{-4}$
		CR	$0.10 \times 10^{-6}$	--	--	--	--	--	--	$1.33 \times 10^{-6}$	$1.61 \times 10^{-6}$
Child	2017-2018	HQ	$6.02 \times 10^{-4}$	$2.60 \times 10^{-4}$	$8.64 \times 10^{-4}$	$11.1 \times 10^{-4}$	$0.81 \times 10^{-4}$	$2.87 \times 10^{-4}$	$7.67 \times 10^{-4}$	$3.73 \times 10^{-2}$	$20.4 \times 10^{-4}$
		CR	$0.08 \times 10^{-6}$	--	--	--	--	--	--	$1.44 \times 10^{-6}$	$1.75 \times 10^{-6}$
	2018-2019	HQ	$5.26 \times 10^{-4}$	$2.17 \times 10^{-4}$	$6.74 \times 10^{-4}$	$11.0 \times 10^{-4}$	$0.57 \times 10^{-4}$	$2.30 \times 10^{-4}$	$7.08 \times 10^{-4}$	$2.95 \times 10^{-2}$	$17.7 \times 10^{-4}$
		CR	$0.07 \times 10^{-6}$	--	--	--	--	--	--	$1.14 \times 10^{-6}$	$1.52 \times 10^{-6}$



2019-2020	HQ	$4.75 \times 10^{-4}$	$1.85 \times 10^{-4}$	$6.27 \times 10^{-4}$	$7.93 \times 10^{-4}$	$0.52 \times 10^{-4}$	$1.70 \times 10^{-4}$	$3.61 \times 10^{-4}$	2.09×	11.4×
									$10^{-2}$	$10^{-4}$
	CR	$0.06 \times 10^{-6}$	--	--	--	--	--	--	0.81×	0.98×
									$10^{-6}$	$10^{-6}$

---



**Table 3** The non-carcinogenic and carcinogenic risks for the deweathered element levels in PM<sub>2.5</sub>.

Age	Year	Indicator	Cr	Mn	Fe	Co	Ni	Cu	Zn	As	Pb
Adult	2017-2018	HQ	$3.07 \times 10^{-4}$	$1.14 \times 10^{-4}$	$3.82 \times 10^{-4}$	$10.3 \times 10^{-4}$	$0.50 \times 10^{-4}$	$1.33 \times 10^{-4}$	$3.15 \times 10^{-4}$	$1.68 \times 10^{-2}$	$10^{-4}$
		CR	$0.16 \times 10^{-6}$	--	--	--	--	--	--	$2.60 \times 10^{-6}$	$3.72 \times 10^{-6}$
	2018-2019	HQ	$2.73 \times 10^{-4}$	$0.96 \times 10^{-4}$	$3.14 \times 10^{-4}$	$4.93 \times 10^{-4}$	$0.35 \times 10^{-4}$	$0.97 \times 10^{-4}$	$2.91 \times 10^{-4}$	$1.22 \times 10^{-2}$	$6.91 \times 10^{-4}$
		CR	$0.14 \times 10^{-6}$	--	--	--	--	--	--	$1.89 \times 10^{-6}$	$2.37 \times 10^{-6}$
	2019-2020	HQ	$2.50 \times 10^{-4}$	$0.82 \times 10^{-4}$	$2.95 \times 10^{-4}$	$3.46 \times 10^{-4}$	$0.36 \times 10^{-4}$	$0.70 \times 10^{-4}$	$1.49 \times 10^{-4}$	$0.78 \times 10^{-2}$	$4.08 \times 10^{-4}$
		CR	$0.13 \times 10^{-6}$	--	--	--	--	--	--	$1.20 \times 10^{-6}$	$1.40 \times 10^{-6}$
Child	2017-2018	HQ	$7.47 \times 10^{-4}$	$2.77 \times 10^{-4}$	$9.28 \times 10^{-4}$	$11.7 \times 10^{-4}$	$1.23 \times 10^{-4}$	$3.22 \times 10^{-4}$	$3.23 \times 10^{-4}$	$4.09 \times 10^{-2}$	$26.4 \times 10^{-4}$
		CR	$0.10 \times 10^{-6}$	--	--	--	--	--	--	$1.58 \times 10^{-6}$	$2.26 \times 10^{-6}$
	2018-2019	HQ	$6.64 \times 10^{-4}$	$2.34 \times 10^{-4}$	$7.64 \times 10^{-4}$	$11.9 \times 10^{-4}$	$0.85 \times 10^{-4}$	$2.36 \times 10^{-4}$	$1.91 \times 10^{-4}$	$2.98 \times 10^{-2}$	$16.8 \times 10^{-4}$
		CR	$0.09 \times 10^{-6}$	--	--	--	--	--	--	$1.15 \times 10^{-6}$	$1.44 \times 10^{-6}$



2019-2020	HQ	$6.08 \times 10^{-4}$	$1.99 \times 10^{-4}$	$7.17 \times 10^{-3}$	$8.42 \times 10^{-4}$	$0.87 \times 10^{-4}$	$1.71 \times 10^{-4}$	$1.34 \times 10^{-3}$	$1.89 \times 10^{-2}$	$9.92 \times 10^{-4}$
									$10^{-2}$	$10^{-4}$
	CR	$0.08 \times 10^{-6}$	--	--	--	--	--	--	$0.73 \times 10^{-6}$	$0.85 \times 10^{-6}$
									$10^{-6}$	$10^{-6}$

---